Evaluation of Perfluorinated Sulfonic Acid Membranes for Vanadium Redox

S S Sha'rani[1,2*], N. W. C. Jusoh[1,2], E Abouzari-Lotf[2,3], A Ahmad[2,3], and R R Ali[1,2]

[1]Malaysia-Japan International Institute of Technology, International Campus, Universiti Teknologi Malaysia, Jalan Semarak 54100, Kuala Lumpur, Malaysia.[2]Advanced Materials Research Group, Center of Hydrogen Energy, Universiti Teknologi Malaysia, Jalan Semarak 54100, Kuala Lumpur, Malaysia.
[3]Department of Chemical Engineering, Universiti Teknologi Malaysia, 81310 Johor Bahru, Malaysia.

*ssophia2@graduate.utm.my

Abstract. The performance and cost of the membranes have always been crucial for the utilization of electrochemical energy devices. This article presents the properties and the performance of two commercially available and low-cost perfluorinated sulfonic acid membranes of GN115 and GN212C for vanadium redox flow battery (VRFB) application in comparison with Nafion117 (N117) membrane. The vanadium (IV) permeability of GN115 membrane was found to be close to N117, unlike GN212C membrane which showed 4 times higher vanadium (IV) permeability than N117 under similar conditions. Both GN115 and GN212C membranes showed isotropic conductivity and higher values than N117. The battery test results indicated that the high coulombic efficiency (CE) and high voltage efficiency (VE) followed the vanadium (IV) permeability and proton conductivity trends. Both membranes revealed outstanding stability in long-term charge-discharge testing under various current densities. The energy efficiency was found to be higher than N117 with values of 76.6% and 76.8% for GN115 and GN212C, respectively. The overall results suggest that both lower-cost membranes have a strong potential for VRFB application as the single-cell performance results were close to N117. The high value of proton conductivity of GN212C membrane compensates its vanadium (IV) permeability leaving reasonable battery performance.

1. Introduction

Vanadium redox flow battery (VRFB) has attracted excessive attention for renewable energy storage due to its unique set of advantages including long life cycle, absence of electrolytes contamination, deep charge and discharge capacity, fast response time, low maintenance cost and relatively large energy and power ratings [1-4]. Compared to traditional rechargeable batteries such as zinc-bromide flow battery and iron-chromium flow battery, VRFB allows the battery's power and capacity to be sized independently. However, widespread commercialization of the battery being postponed due to the high capital cost. Such high cost is mainly attributed to the cost of components' materials including membranes [5]. Therefore, developing low-cost membranes is one of the major challenges to prompt the development of high-performance energy storage systems.

In VRFB, the membrane acts as a barrier to prohibit the undesired permeability of negative and positive electrolytes and transfer protons during the passage of current [1, 6]. Therefore, to achieve a high-performance battery, the membrane needs to possess low vanadium permeability without

scarifying the desired proton conductivity and excellent mechanical and chemical stability in harsh acidic electrolytes in addition to having an affordable cost. Currently, perfluorinated sulfonic acid (PFSA) membranes representing by Nafion® are the most widely used material in VRFB, displaying outstanding mechanical and chemical stability and high conductivity [8-11]. However, despite its desired advantages, Nafion based membranes are challenged by high vanadium ion crossover in addition to high cost [7, 8]. Undesired crossover leads to a reduction in coulombic efficiency due to the self-discharge phenomenon [9]. This situation further emphasizes the need for the development of new alternative cost-effective membranes to prompt the mass deployment of VRFB technology in the market place.

The majority of newly researched membranes for VRFB are hydrocarbon-based materials [10-15]. Typically, sulfonated aromatic polymers based on poly(ether ether ketone) [16-18], poly(fluorenyl ether ketone)s [13, 14], polysulfones [12, 19], poly(arylene ether sulfone)s [12, 20, 21] and poly(phthalazinone ether ketone ketone)s [22, 23] were developed and tested in the battery. Although some improvements have been achieved, most of these new membranes did not meet all requirements for commercial applications. Particularly, the polar groups of the membranes are not stable enough in the highly oxidative environment of the battery [24-26]. Moreover, most of these membranes are prepared in a lengthy multistep procedure that adversely affects the cost-effectiveness [5, 14]. Therefore, it seems that the technically and industrially viable alternative to improve the battery performance is the use of commercially available and low-cost ion exchange materials with established technology.

In this work, two newly developed low-cost commercial PFSA membranes named as GN115 and GN212C were investigated for application in VRFB. Unlike Nafion117, these membranes were manufactured through the casting method instead of extrusion. The structures and properties of the membranes were initially investigated using Scanning Electron Microscopy (SEM), X-Ray Diffraction (XRD), Fourier Transform Infrared (FTIR) spectroscopy and Thermal Analysis (TGA). The efficiency of the membranes was evaluated through vanadium ion permeability and proton conductivity analysis. The preliminary behavior of the membranes in VRFB was also studied using a single cell test in comparison to Nafion 117.

2. Experimental section

2.1. Materials

The GN115 and GN212C membranes with thickness of 115 and 33 μm were provided in-kind by General Energy, Co., Ltd. GN212C is a composite membrane with special graphene formula. N117 (177 μm) was selected for comparison in this study due to the well-balanced properties of vanadium permeability and conductivity among other Nafion series. Vanadium (IV) oxide sulfate hydrate, $VOSO_4.nH_2O$ of 97% purity was purchased from Sigma Aldrich. The other chemicals used in this work were purchased from Mallinckrodt Baker. The as-received GN115 and GN212C membranes were pretreated according to the standard protocol used for N117 membrane. This involved immersion of the membranes in 3 wt. % H_2O_2 solution for 1 h at 100 ℃ followed by immersion in distilled water for 1 h at 100 ℃ and immersion in 2.0 M H_2SO_4 solution for 1 hour at 100 ℃. Finally, the membranes were immersed in distilled water for 1 h at 100 ℃ and kept in the distilled water prior to use.

2.2 Membrane Characterization

The infrared spectra were recorded on Perkin Elmer FTIR spectrophotometer (Spectrum 100) at wave number range 600–4000 cm^{-1}. XRD of the membranes were performed on PANatytic XPert Pro (λ = 0.15406 nm) at 45 kV and 20 mA and diffraction angle range of 2 θ = 10–80° with 2° min^{-1}. Thermal degradation of the membranes was recorded on a TGA Q50 (TA Instruments). Prior to the analysis, the membranes were vacuum-dried at 60 ℃ overnight and analysed with a 10 ℃ min^{-1} heating rate under N_2 atmosphere. Scanning Electron Microscope of GEMINI500 was used to evaluate the surface morphology of the membranes. Prior to imaging, the membranes were coated with Platinum by using Auto-fine coater (JEC-3000FC, JEOL, Japan) for 30 s at 20 mA.

The in-plane ($\boldsymbol{\sigma}_{\parallel}$)and through-plane ($\boldsymbol{\sigma}_{\perp}$) proton conductivity values of the membranes were recorded by BekkTech conductivity (BT-112, four-point probe) and home-made cells, respectively as shown in Figure 1. The home-made cell used stainless steel electrodes freshly polished with a diamond polishing machine. The membranes were tested by clamping in the cells and subsequently immersing in a beaker of 1.0 M H_2SO_4 at room temperature. A DC conductivity testing (Keithley Kickstart SMU 2400) was set to provide the voltage between the central probes and to measure the resulting current in the membrane. The resistance (R) obtained from the slope of voltage versus current plot and the proton conductivity (σ) were calculated by using equation 1:

$$\sigma(\mathrm{S/cm}) = \frac{\mathrm{L\ (cm)}}{\mathrm{R(\Omega)xA(cm^2)}} \tag{1}$$

where A is the area of the membranes and L is the distance between the two inner probes. The denominator of the equation is the area times resistance (AR). Anisotropic proton conductivity ratio was calculated from the values of conductivity obtained by in-plane and through-plane methods according to equation 2.

$$\boldsymbol{\sigma}_{\parallel/\perp} = \frac{\boldsymbol{\sigma}_{\parallel}}{\boldsymbol{\sigma}_{\perp}} \tag{2}$$

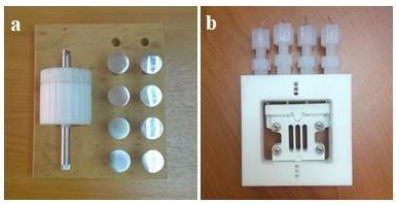

Figure 1. Conductivity cells for (a) trough-plane and (b) in-plane measurements

The permeability of vanadium (IV) across the membranes was measured with the method described elsewhere [11]. The membrane with an effective area of 1.72 cm^2 was clamped in a side-bi-side cell (Perme Gear, Inc.). The left side of the cell was filled with 1.0 M $VOSO_4$ in 2.5 M H_2SO_4 solution while the right side was filled with 1.0 Na_2SO_4 in 2.5 M H_2SO_4 solution. The solution in the right side was termed as blank solution. The solutions in both half-cells were continuously stirred at 220 RPM to avoid concentration polarization. UV-Vis spectrophotometer (UV-1800 Shimadzu) was used to monitor the concentration of permeated vanadium ion. The permeability of the vanadium ion (*P*) was obtained from the slope of the plot of the vanadium (IV) concentration ($C_{V(IV)}$) versus diffusion time (*t*) using equation 3.

$$\boldsymbol{C_{V(IV)} = \frac{AP}{V_R T} C_L (t - t_0)} \tag{3}$$

where, t_0 and C_0 are the initial time and vanadium (IV) concentration in the right side of the cell, V_R is the total volume of solutions. *T* and *A* are the thickness and membrane effective area, respectively. The selectivity of ion transport in the membrane is defined as the ratio of proton conductivity and vanadium permeability.

2.3 VRFB single cell performance

The VRFB single cell was assembled by clamping the membrane with two carbon felts (5 cm x 5 cm), two PVC plates and two rubber sheets to provide the necessary pressure. The electrolyte of 1.5 $m^{V3.5+}$ (m_{VO}^{2+}= m_V^{3+}) in 3.0 m H_2SO_4 solution was used for positive and negative sides [27]. The volume of the electrolytes on each side was 22 mL and both electrolytes were cyclically pumped from

the storage tank into respective half-cells with a flow rate of 10 mL min^{-1}. The temperature of the electrolytes and the cell was kept at 30 °C. The charge-discharged tests were performed under the same operating conditions and controlled by a battery testing system (MTI-BST8) with a cut-off voltage of 1.72 V and 0.8 V. Voltage efficiency (VE), coulombic efficiency (CE) and energy efficiency (EE) for a single charge-discharge cycle were calculated as follows [21, 23]:

$$CE = \frac{I_{constant} t_{discharge}}{I_{constant} t_{charge}} \times 100\% \quad (4)$$

$$VE = \frac{V_{discharge}}{V_{charge}} \times 100\% \quad (5)$$

$$EE = CE \times VE \quad (6)$$

3. Results and discussion

3.1 Characterization of membranes

The IR spectra for GN115 and GN212C membranes is shown in the Figure 2. The peaks between 1000 and 1360 cm^{-1} are attributed to the C-F absorption related bonds. Peaks at 1060 and 976 cm^{-1} represent the S–O and C–O–C groups of the PFSAs, respectively. The peak at 1637 cm^{-1} is assigned to the bending vibration of O–H due to absorbed water. It can be seen that the spectra of GN115 and GN212C membranes are identical to N117 representing perfluorinated sulfonic acid membranes and the band positions are in a good agreement with the literature values [28-30].

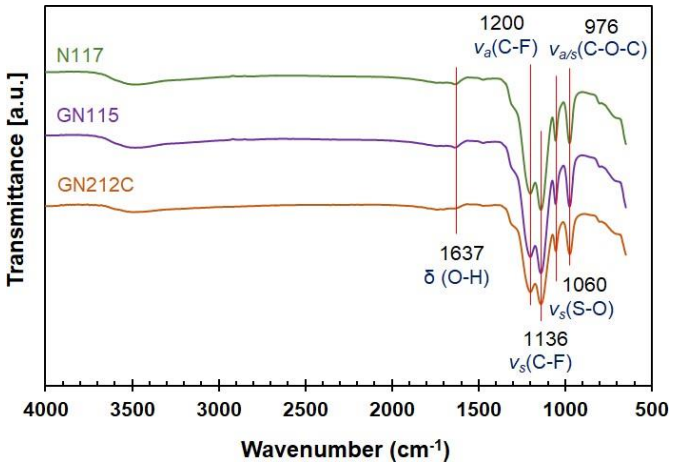

Figure 2. FT-IR spectra of GN115, GN212C and N117 membranes

The XRD curves of GN115, GN212C membranes are displayed in Figure 3 is compared with N117. The peak at 2 θ of 16–18˚ and the halo at 37–40˚, shown in all membranes, are attributed to the PTFE-like backbone and amorphous structure of the PFSA type membranes, respectively [31]. Comparing the curves of N117, GN115 and GN212C reveals that the GN212C has slightly higher peak intensity at 22˚. Such minor difference could be ascribed to the presence of graphene in the GN212C composite membrane [32, 33].

The TGA curves of GN115, GN212C and N117 membranes are shown in Figure 3a. The TGA curves of the GN115 seem to be similar to that of N117 and overlapping. Unlikely, the GN212C membrane shows a slightly different curve with the thermal degradation started at lower temperature compared to N117. This slightly lower thermal stability of GN212C composite membrane could be due to the introduction of graphene filler [34].

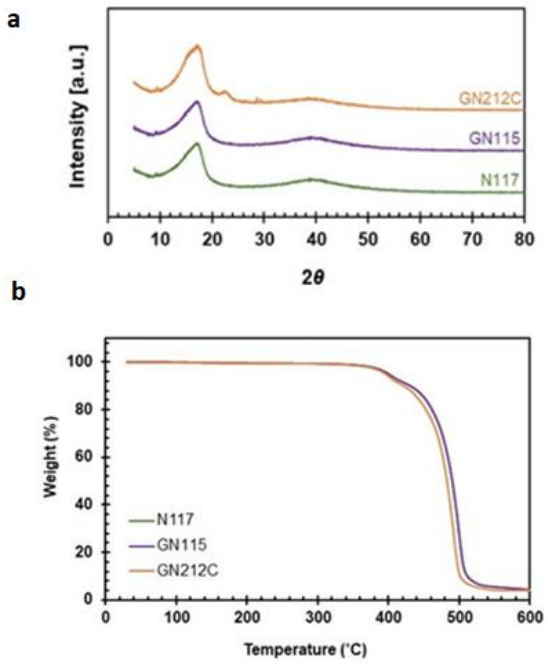

Figure 3. XRD (a) and TGA (b) curves of GN115 and GN212C membranes in comparing with N117

The surface morphology of the membranes was evaluated using SEM as shown in the Figure 4. Comparison of the SEM images of N117 with GN115 and GN212C membranes indicates that the casted membranes of GN212C and GN115 membranes have a rougher surface in compared to the N117.

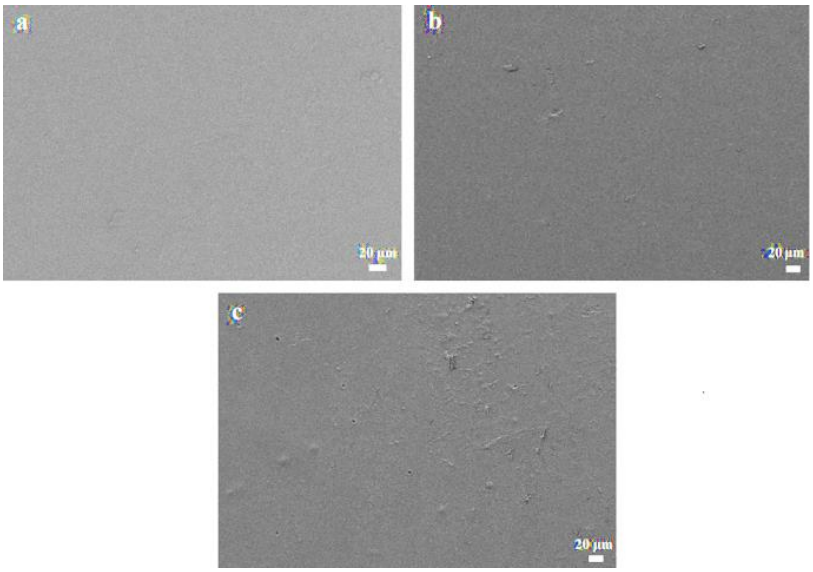

Figure 4. The surface SEM images of N117(a), GN115 (b) and GN212C (c) membranes.

3.2 Proton Conductivity, vanadium ion permeability and selectivity

To investigate the overall efficiency of the membranes in VRFB, proton conductivity, vanadium ion permeability and the single cell tests were evaluated and compared with N117. As shown in the Table 1, both of these low-cost PFSAs showing higher conductivity values and lower area resistance than N117. The composite GN212C is showing considerably higher conductivity values of as high as 108 mS cm^{-1} at room temperature. This remarkable high conductivity value is possibly due to the lower thickness and introducing of graphene-based filler. Area resistance is an imperative parameter that determine the voltage efficiency of the VRFB [1]. Therefore, the results give a good indication that the membranes could perform better than N117 in VRFB. Comparing the through-plane and in-plane conductivity values of these new PFSAs were performed to clarify the isotropic or anisotropic behaviour. The conductivity values for N117 showed anisotropic behaviour with comparable levels with the reported values of through-plane and in-plane [35, 36]. In contrast, both GN212C and GN115 show almost isotropic conductivity as only slightly differences in the through-plane and in-plane conductivity values were observed. As reported in the literature, the anisotropic proton conductivity of PFSAs is mainly depends on the membrane preparation and pre-treatment such as casting, stretching, extrusion and hot-pressing [37-40]. It could be concluded that the collection of isotropic grains is randomly oriented in the GN212C and GN115 membranes upon solution casting assisted film preparation. Whereas, the conducting domains are mainly in the plane or perpendicular to the plane of the film in Nafion117 [41].

Different vanadium ions of V^{2+}, V^{3+}, VO^{2+}, and VO_2^{+} are present in a VRFB electrolyte. Permeability of VO^{2+} was evaluated to observe the trends in the new low-cost PFSAs in comparison to N117. The permeability was measured using side-bi-side cell at room temperature. Prior to the measurement, a standard curve of VO^{2+} was established using UV- Vis spectrophotometry technique and the peak of VO^{2+} was recorded at 765 nm. Figure 5 shows the plot for the variation of VO^{2+} concentration in the blank solution after crossing different membranes as a function of time. Among all membranes, GN212C showed the highest VO^{2+} permeability of 95.5 ×10–7 $cm^2.min^{-1}$ which is almost 4 times higher than the values for GN115 and N117. On the other hand, the permeability of GN115 was close to N117. In fact, the composition, fabrication procedure and thickness of the membranes are controlling the vanadium permeability. In general, membranes prepared by extrusion are showing high degree of amorphous structure which results in larger fractional free volume and higher vanadium permeability than casted membranes. The extent of fabrication procedure on the permeability could be reduced due the pre-treatments of soaking in acid and water as well as exposure to electrolyte. The permeability increase trend of GN212C > GN115 > N117 that the differences in the membrane thickness and possibly microstructures are dominating the electrolyte permeability. Therefore, it is reasonable to state that the increase in the thickness cause a gradual decrease in the VO^{2+} permeability. This is due to the longer and more complicated transfer channels in thicker membranes.

The ion selectivity of the membranes, which is the ratio of proton conductivity over vanadium ion permeability, was investigated to allow an efficient determination of membrane appropriateness for VRFB that goes beyond the routine determination of the conductivity and electrolyte permeability. A higher value for ion selectivity implies enhanced performance of the membrane in VRFB. Table 1 summarizes the data for ion selectivity together with the proton conductivity, area resistance and vanadium permeability of the new PFSA membranes compared to N117. The area resistance of the membrane was calculated based on the through-plane value. The highest ion selectivity of 3.84×10^4 S min cm^{-3} was calculated for GN115 membrane which is substantially higher than the values of N117 and GN212C membranes. This confirms that the GN115 membrane has a good balance between the vanadium (VO^{2+}) permeability and the proton conductivity.

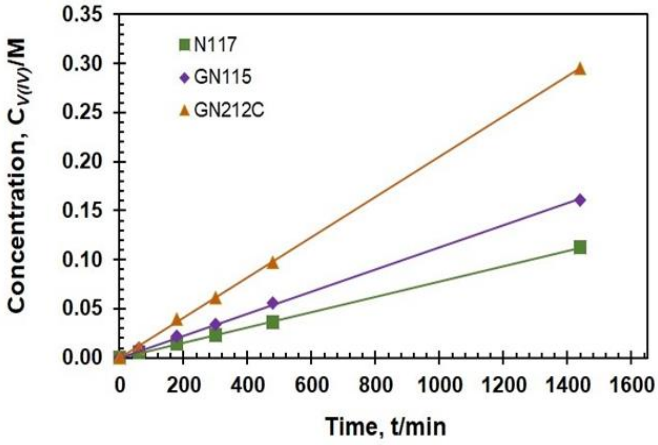

Figure 5. Time-dependent variation of VO^{2+} concentration in blank solution across the investigated membranes.

Table 1. Proton conductivity, area resistance, VO^{2+} permeability and ionic selectivity of the membranes.

Membrane	Thickness, (μm)	Proton conductivity, σ (mS/cm)		Area Resistance (Ω cm²)	Vanadium permeability (x10⁻⁷ cm² min⁻¹)	Ion selectivity (x10⁴ S min cm⁻³)
		Through-plane ($\sigma_{\perp}$)	In-plane ($\sigma_{\parallel}$)			
GN115	115	96.1	96.0	0.12	25.0	3.84
GN212C	33	108.3	108.5	0.03	95.5	1.14
Nafion 117	177	88.0	82.6	0.20	24.0	3.52

3.3 VRFB single cell performance

The cycling performance of the battery assembled with both membranes was investigated using a charge-discharge test at current densities of 40, 60, 80 and 120 mA cm^{-2} for 10 cycles in compared with commercial N117. As shown in the typical charge-discharge cycles at 40 mA.cm^{-2} (Figure 6), both GN115 and GN212C membranes have good and stable performance in VRFB as of N117. Such cycling data were used to calculate the cell efficiency parameters of CE, VE and EE. Figure 7 shows typical efficiency parameters for the membranes at 40 mA cm^{-2}. At this current density, GN115 membrane shows the highest CE of 89.5% and highest VE of 88.2% was achieved for GN212C membrane. Substantially improvements in the CE and VE of GN115 and GN212C membranes could be attributed to the is mainly due to lower vanadium crossover in GN115 and area resistance in GN212C, respectively. In fact, very high vanadium permeability and very low area resistance of GN212C are direct consequences of membrane thickness. On the other hand, the EE of GN115 and GN212C was found to be close to N117 at 40 mA cm^{-2}, suggesting a high potential of these low-cost membranes due to the proper balance between the proton conductivity and the vanadium permeability.

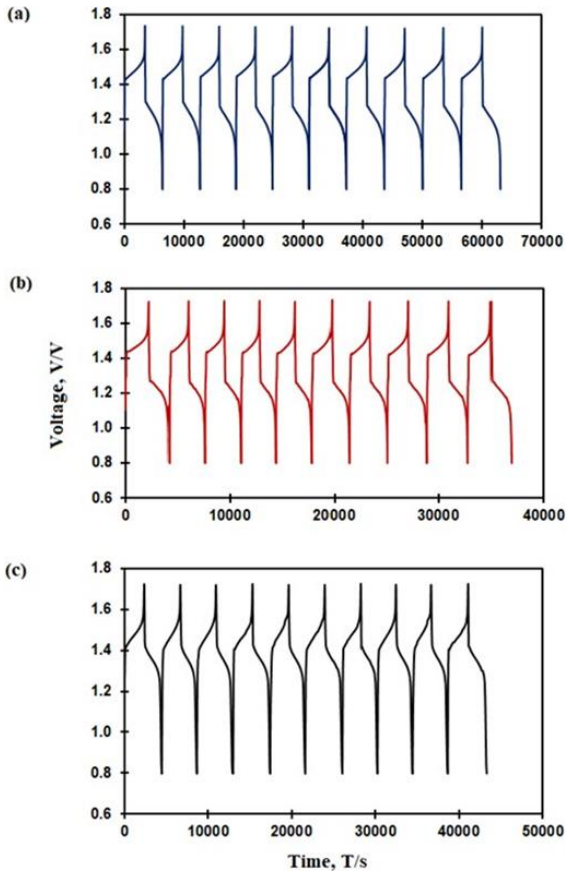

Figure 6. Comparison of the charge-discharge cycles of N117 (a), GN115 (b) and GN212C (c) membranes at 40 mA cm^{-2}.

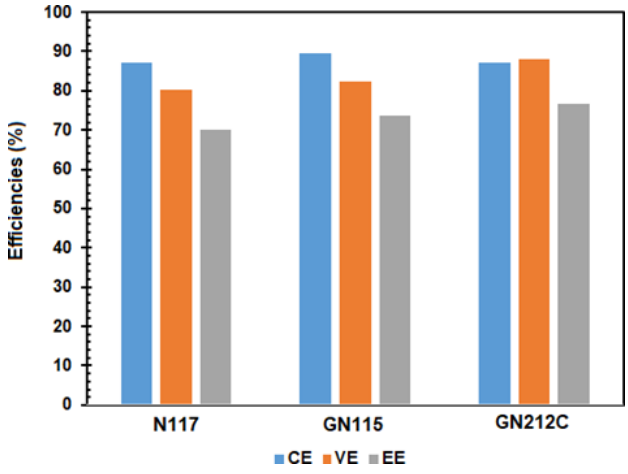

Figure 7. Efficiencies of the VRB employing low-cost PFSA membranes in compared to N117 at 40 mA cm^{-2}.

In order to evaluate the chemical and electrochemical stability of these two new membranes over long time and higher current densities, 10 cycles of charge-discharge test were conducted at each current density of 40, 60, 80 and 120 mA cm^{-2}. Stable CE, VE and EE values were obtained and the average values for the parameters were plotted in Figure 8.

In general, all membranes show increased in CE when the current density value increased. At lowest current density, the CE of GN115 is slightly higher than N117, however the CE value of N117 overtake the CE value of GN115 when the current density increased to 60 mA cm^{-2}. The CE of the membranes is greater at higher current density due to shorter time required to achieve an equal state of charge [42]. In comparison to the reported membranes in the literature, average CE was comparable. Typically, the CE of GN115 is higher than Nafion 115 [43] and porous polyvinylidene fluoride membranes [44] at 80 mA cm^{-2} and sulfonated poly(ether ether ketone) (SPEEK) at 40 mA cm^{-2} [45]. Unlike CE, the values of VE decreased rapidly when the current density is increased. This can be due to a higher ohmic losses when applying higher current. In addition, the values for EE of N117, GN115 and GN212C decreased steadily with higher current density due to the decreased in the VE. From the results, it can be concluded that the major factor for the EE of the membranes, comes from value of VE. However, the EE is still comparable with diverse cation exchange membranes reported in the literature e.g. N115, N112, N1135 [43], sulfonated polyimide [46] amphoteric ion exchange membrane [47] and SPEEK [45, 48]. Generally, the results show that the both low-cost PFSA membranes have excellent stability and good performance in the redox flow battery and can be employed in industrial applications.

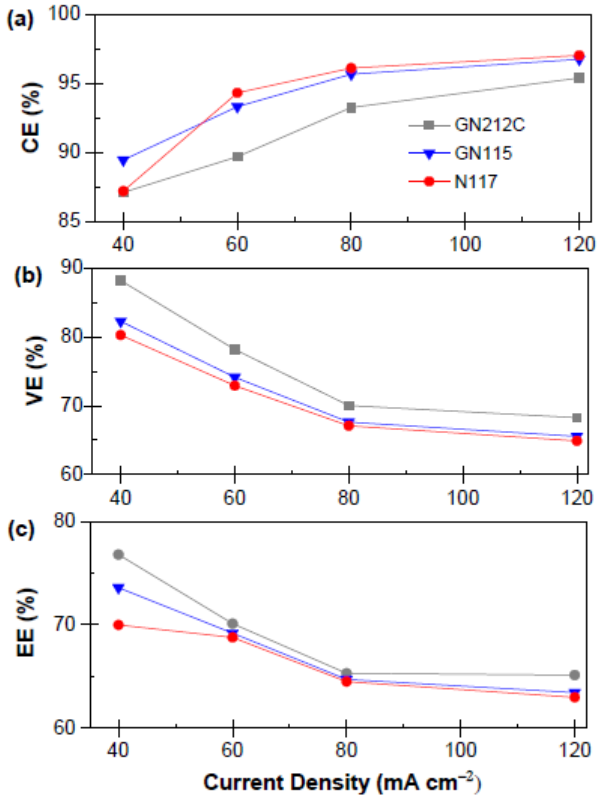

Figure 8. Cyclic performance of the VRB single cell assembled N117, GN115 and GN212C.

4. Conclusion

In this work, newly commercialized low-cost perfluorinated sulfonic acid membranes of GN115 and GN212C were investigated for potential VRFB application in comparison with well-established N117 membrane. The presence of graphene filler in GN212C membrane was led to an obvious enhancement in its conductivity. The results of SEM revealed that these new solution casted membranes have more roughed surface compared to the N 117. The GN212C membrane showed the highest proton conductivity compared to both N117 and GN115 membranes. The GN115 membrane showed a vanadium permeability of at par with N117 membrane. Although GN212C membrane has the highest

vanadium permeability, the high proton conductivity and small area resistance can still be considered for VRFB application. The efficiencies of the GN115 and GN212C at 40 $mA.cm^{-2}$ were also close to the N117 suggesting a strong potential for the membrane to be used in VRFB.

Acknowledgment
The authors wish to acknowledge the financial support from Fundamental Research Grant (FRGS) awarded by Ministry of higher education (Vot.#4F775). The authors also wish to thank General Energy Co., Ltd for providing the samples of GN212C and GN115 membranes.

References

[1] B. Schwenzer, J. Zhang, S. Kim, L. Li, J. Liu, Z. Yang 2011 Membrane development for vanadium redox flow batteries, *ChemSusChem* **4** 1388-1406
[2] A.Z. Weber, M.M. Mench, J.P. Meyers, P.N. Ross, J.T. Gostick, Q.H. Liu 2011 Redox flow batteries: a review *Journal of Applied Electrochemistry* **41** 1137-1164
[3] L.H. Yu, F. Lin, L. Xu, J.Y. Xi 2016 A recast Nafion/graphene oxide composite membrane for advanced vanadium redox flow batteries, *Rsc Advances* **6** 3756-3763
[4] R. Ye, D. Henkensmeier, S.J. Yoon, Z. Huang, D.K. Kim, Z. Chang, S. Kim, R. Chen 2017 Redox Flow Batteries for Energy Storage: A Technology Review *Journal of Electrochemical Energy Conversion and Storage* **15** 010801-010801-010821.
[5] R. Ye, D. Henkensmeier, S.J. Yoon, Z. Huang, D.K. Kim, Z. Chang, S. Kim, R. Chen 2017 Redox Flow Batteries for Energy Storage: A Technology Review *Journal of Electrochemical Energy Conversion and Storage* **15** 2017
[6] L. Cao, A. Kronander, A. Tang, D.W. Wang, M. Skyllas-Kazacos 2016 Membrane Permeability Rates of Vanadium Ions and Their Effects on Temperature Variation in Vanadium Redox Batteries *Energies* **9** 2016
[7] G.-J. Hwang, S.-W. Kim, D.-M. In, D.-Y. Lee, C.-H. Ryu 2018 Application of the commercial ion exchange membranes in the all-vanadium redox flow battery *Journal of Industrial and Engineering Chemistry* **60** 360-365
[8] J. Vrána, J. Charvát, P. Mazúr, P. Bělský, J. Dundálek, J. Pocedič, J. Kosek 2018 Commercial perfluorosulfonic acid membranes for vanadium redox flow battery: Effect of ion-exchange capacity and membrane internal structure *Journal of Membrane Science* **552** 202-212
[9] J. Dai, Y. Dong, P. Gao, J. Ren, C. Yu, H. Hu, Y. Zhu, X. Teng 2018 A sandwiched bipolar membrane for all vanadium redox flow battery with high coulombic efficiency *Polymer* **140** 233-239
[10] I. Strużyńska-Piron, M. Jung, A. Maljusch, O. Conradi, S. Kim, J.H. Jang, H.-J. Kim, Y. Kwon, S.W. Nam, D. Henkensmeier 2017 Imidazole based ionenes, their blends with PBI-OO and applicability as membrane in a vanadium Redox flow battery *European Polymer Journal* **96** 383-392
[11] S.S. Sha'rani, E.A. Lotf, A. Ahmad, W.A.W. Ibrahim, M.M.E.-s. Nasef, R.R. Ali 2016 Stability and performance evaluation of ion-exchange membranes for vanadium redox flow battery *Jurnal Teknologi* **78** 7-12
[12] S.-W. Choi, T.-H. Kim, S.-W. Jo, J.Y. Lee, S.-H. Cha, Y.T. Hong 2018 Hydrocarbon membranes with high selectivity and enhanced stability for vanadium redox flow battery applications: Comparative study with sulfonated poly(ether sulfone)s and sulfonated poly(thioether ether sulfone)s *Electrochimica Acta* **259** 427-439
[13] Y. Wang, S. Wang, M. Xiao, D. Han, M.A. Hickner, Y. Meng 2013 Layer-by-layer self- assembly of PDDA/PSS-SPFEK composite membrane with low vanadium permeability for vanadium redox flow battery *RSC Advances* **3** 15467
[14] W.M. Xie, R.X. Zheng, X. Song, F.C. Ding, X.H. Huang, Q.D. Ling 2014 Sulfonated Poly(fluorenyl ether ketone) Membranes with Suppressed Semi-Interpenetrating Crossover

and Enhanced Proton Selectivity for Vanadium Redox Flow Batteries *Advanced Materials Research* **1004-1005** 692-695.

[15] J. Liao, Y. Chu, Q. Zhang, K. Wu, J. Tang, M. Lu, J. Wang 2017 Fluoro-methyl sulfonated poly(arylene ether ketone- co -benzimidazole) amphoteric ion-exchange membranes for vanadium redox flow battery *Electrochimica Acta* **258** 360-370

[16] D.H. Hyeon, J.H. Chun, C.H. Lee, H.C. Jung, S.H. Kim 2015 Composite membranes based on sulfonated poly(ether ether ketone) and SiO2 for a vanadium redox flow battery *Korean Journal of Chemical Engineering* **32** 1554-1563

[17] H.Y. Jung, S. Jeong, Y. Kwon 2016 The Effects of Different Thick Sulfonated Poly (Ether Ether Ketone) Membranes on Performance of Vanadium Redox Flow Battery *Journal of the Electrochemical Society* **163** A5090-A5096

[18] F. Wang, G. Wang, J. Zhang, B. Li, J. Zhang, J. Deng, J. Chen, R. Wang 2017 Novel sulfonated poly(ether ether ketone)/oxidized g-C 3 N 4 composite membrane for vanadium redox flow battery applications *Journal of Electroanalytical Chemistry* **797** 107-112

[19] B.P. Gindt, Z.J. Tang, D.L. Watkins, D.G. Abebe, S. Seo, S. Tuli, H. Ghassemi, T.A. Zawodzinski, T. Fujiwara 2017 Effects of sulfonated side chains used in polysulfone based PEMs for VRFB separator *Journal of Membrane Science* **532** 58-67

[20] L. Semiz, N.D. Sankir, M. Sankir 2014 Directly Copolymerized Disulfonated Poly(arylene ether sulfone) Membranes for Vanadium Redox Flow Batteries *Int. J. Electrochem. Sc*. **9** 3060-3067

[21] D.Y. Chen, S.J. Wang, M. Xiao, Y.Z. Meng 2010 Synthesis and properties of novel sulfonated poly(arylene ether sulfone) ionomers for vanadium redox flow battery *Energ Convers Manage* **51** 2816-2824

[22] B.G. Zhang, S.H. Zhang, D.B. Xing, R.L. Han, C.X. Yin, X.G. Jian 2012 Quaternized poly(phthalazinone ether ketone ketone) anion exchange membrane with low permeability of vanadium ions for vanadium redox flow battery application *Journal of Power Sources* **217** 296-302.

[23] S.H. Zhang, B.G. Zhang, D.B. Xing, X.G. Jian 2013 Poly(phthalazinone ether ketone ketone) anion exchange membranes with pyridinium as ion exchange groups for vanadium redox flow battery applications *J. Mater. Chem. A* **1** 12246-12254.

[24] S. Kim, T.B. Tighe, B. Schwenzer, J. Yan, J. Zhang, J. Liu, Z. Yang, M.A. Hickner 2011 Chemical and mechanical degradation of sulfonated poly(sulfone) membranes in vanadium redox flow batteries *Journal of Applied Electrochemistry* **41** 1201-1213

[25] Z. Yuan, X. Li, J. Hu, W. Xu, J. Cao, H. Zhang 2014 Degradation mechanism of sulfonated poly(ether ether ketone) (SPEEK) ion exchange membranes under vanadium flow battery medium *Physical chemistry chemical physics : PCCP* **16** 19841-19847

[26] Z. Yuan, X. Li, Y. Zhao, H. Zhang 2015 Mechanism of Polysulfone-Based Anion Exchange Membranes Degradation in Vanadium Flow Battery *ACS applied materials & interfaces* **7** 19446-19454

[27] M. Etesami, E. Abouzari-Lotf, A. Ripin, M. Mahmoud Nasef, T.M. Ting, A. Saharkhiz, A. Ahmad 2018 Phosphonated graphene oxide with high electrocatalytic performance for vanadium redox flow battery *International Journal of Hydrogen Energy* **43** 189-197

[28] K. Feng, L. Hou, B. Tang, P. Wu 2015 Does thermal treatment merely make a H2O-saturated Nafion membrane lose its absorbed water at high temperature? *Physical chemistry chemical physics : PCCP* **17** 9106-9115

[29] J. Grosse Austing, C. Nunes Kirchner, L. Komsiyska, G. Wittstock 2016 Layer-by-layer modification of Nafion membranes for increased life-time and efficiency of vanadium/air redox flow batteries *Journal of Membrane Science* **510** 259-269

[30] Z. Liang, W. Chen, J. Liu, S. Wang, Z. Zhou, W. Li, G. Sun, Q. Xin 2004 FT-IR study of the microstructure of Nafion® membrane *Journal of Membrane Science* **233** 39-44

[31] T. Li, G.M. Zhong, R.Q. Fu, Y. Yang 2010 Synthesis and characterization of Nafion/cross- linked PVP semi-interpenetrating polymer network membrane for direct methanol fuel cell *Journal of Membrane Science* **354** 189-197
[32] C.F. Chang, Q.D. Truong, J.R. Chen 2013 Graphene as excellent support for rapid and efficient near infrared-assisted tryptic proteolysis *Colloids and surfaces. B, Biointerfaces* **104** 221-228
[33] J. Ding, W. Yan, W. Xie, S. Sun, J. Bao, C. Gao 2014 Highly efficient photocatalytic hydrogen evolution of graphene/YInO3 nanocomposites under visible light irradiation *Nanoscale* **6** 2299-2306
[34] R. Kumar, M. Mamlouk, K. Scott 2011 A Graphite Oxide Paper Polymer Electrolyte for Direct Methanol Fuel Cells *International Journal of Electrochemistry* **2011** 1-7.
[35] M.W. Verbrugge 1990 Analysis of Promising Perfluorosulfonic Acid Membranes for Fuel-Cell Electrolytes *Journal of The Electrochemical Society* **137** 3770
[36] N. Yoshida, T. Ishisaki, A. Watakabe, M. Yoshitake 1998 Characterization of Flemion® membranes for PEFC *Electrochimica Acta* **43** 3749-3754
[37] T. Soboleva, Z. Xie, Z. Shi, E. Tsang, T. Navessin, S. Holdcroft 2008 Investigation of the through-plane impedance technique for evaluation of anisotropy of proton conducting polymer membranes *Journal of Electroanalytical Chemistry* **622** 145-152
[38] K.A. Mauritz, R.B. Moore 2004 State of understanding of Nafion *Chemical reviews* **104** 4535-4586
[39] J. Hou, J. Li, K.G. Wilmsmeyer, Z. Zhang, L.A. Madsen 2011 Understanding Anisotropy, Transport, and Ion Associations Inside Ionic Polymers, in: NMR Spectroscopy of Polymers: Innovative Strategies for Complex Macromolecules *American Chemical Society* **2011** 251-263
[40] J.K. Park, J. Li, G.M. Divoux, L.A. Madsen, R.B. Moore 2011 Oriented Morphology and Anisotropic Transport in Uniaxially Stretched Perfluorosulfonate Ionomer Membranes *Macromolecules* **44** 5701-5710
[41] M.J. Park, N.P. Balsara 2010 Anisotropic Proton Conduction in Aligned Block Copolymer Electrolyte Membranes at Equilibrium with Humid Air *Macromolecules* **43** 292-298
[42] Y. Li, J. Sniekers, J.C. Malaquias, C. Van Goethem, K. Binnemans, J. Fransaer, I.F.J. Vankelecom 2018 Crosslinked anion exchange membranes prepared from poly(phenylene oxide) (PPO) for non-aqueous redox flow batteries *Journal of Power Sources* **378** 338-344
[43] B. Jiang, L. Wu, L. Yu, X. Qiu, J. Xi 2016 A comparative study of Nafion series membranes for vanadium redox flow batteries *Journal of Membrane Science* **510** 18-26
[44] W. Wei, H. Zhang, X. Li, H. Zhang, Y. Li, I. Vankelecom 2013 Hydrophobic asymmetric ultrafiltration PVDF membranes: an alternative separator for VFB with excellent stability *Physical chemistry chemical physics : PCCP* **15** 1766-1771
[45] S. Winardi, S.C. Raghu, M.O. Oo, Q. Yan, N. Wai, T.M. Lim, M. Skyllas-Kazacos 2014 Sulfonated poly (ether ether ketone)-based proton exchange membranes for vanadium redox battery applications *Journal of Membrane Science* **450** 313-322
[46] J. Li, X. Yuan, S. Liu, Z. He, Z. Zhou, A. Li 2017 A Low-Cost and High-Performance Sulfonated Polyimide Proton-Conductive Membrane for Vanadium Redox Flow/Static Batteries *ACS applied materials & interfaces* **9** 32643-32651
[47] J. Qiu, M. Zhai, J. Chen, Y. Wang, J. Peng, L. Xu, J. Li, G. Wei 2009 Performance of vanadium redox flow battery with a novel amphoteric ion exchange membrane synthesized by two-step grafting method *Journal of Membrane Science* **342** 215-220
[48] R. Gan, Y. Ma, S. Li, F. Zhang, G. He 2017 Facile fabrication of amphoteric semi-interpenetrating network membranes for vanadium flow battery applications *Journal of Energy Chemistry* **2017**